2011

Locomotor loading mechanics in the hindlimbs of tegu lizards (Tupinambis merianae): Comparative and evolutionary implications

K. Megan Sheffield, *University of South Florida*
Michael T. Butcher, *Youngstown State University*
S. Katharine Shugart, *Clemson University*
Jennifer C. Gander, *Clemson University*
Richard W. Blob, *Clemson University*

The Journal of Experimental Biology 214, 2616-2630

doi:10.1242/jeb.048801

RESEARCH ARTICLE

Locomotor loading mechanics in the hindlimbs of tegu lizards (*Tupinambis merianae*): comparative and evolutionary implications

K. Megan Sheffield[1,*], Michael T. Butcher[2], S. Katherine Shugart[1], Jennifer C. Gander[1,†] and Richard W. Blob[1,‡]

[1]Department of Biological Sciences, Clemson University, Clemson, SC 29634, USA and [2]Department of Biological Sciences, Youngstown State University, OH 44555, USA

*Present address: Department of Academic Services, University of South Florida, Tampa, FL 33620, USA
†Present address: Department of Epidemiology and Biostatistics, Arnold School of Public Health, University of South Carolina, Columbia, SC 29208, USA
‡Author for correspondence (rblob@clemson.edu)

Accepted 9 May 2011

SUMMARY

Skeletal elements are usually able to withstand several times their usual load before they yield, and this ratio is known as the bone's safety factor. Limited studies on amphibians and non-avian reptiles have shown that they have much higher limb bone safety factors than birds and mammals. It has been hypothesized that this difference is related to the difference in posture between upright birds and mammals and sprawling ectotherms; however, limb bone loading data from a wider range of sprawling species are needed in order to determine whether the higher safety factors seen in amphibians and non-avian reptiles are ancestral or derived conditions. Tegus (family Teiidae) are an ideal lineage with which to expand sampling of limb bone loading mechanics for sprawling taxa, particularly for lizards, because they are from a different clade than previously sampled iguanas and exhibit different foraging and locomotor habits (actively foraging carnivore *versus* burst-activity herbivore). We evaluated the mechanics of locomotor loading for the femur of the Argentine black and white tegu (*Tupinambus merianae*) using three-dimensional measurements of the ground reaction force and hindlimb kinematics, *in vivo* bone strains and femoral mechanical properties. Peak bending stresses experienced by the femur were low (tensile: 10.4±1.1 MPa; compressive: –17.4±0.9 MPa) and comparable to those in other reptiles, with moderate shear stresses and strains also present. Analyses of peak femoral stresses and strains led to estimated safety factor ranges of 8.8–18.6 in bending and 7.8–17.5 in torsion, both substantially higher than typical for birds and mammals but similar to other sprawling tetrapods. These results broaden the range of reptilian and amphibian taxa in which high femoral safety factors have been evaluated and further indicate a trend for the independent evolution of lower limb bone safety factors in endothermic taxa.

Key words: locomotion, biomechanics, evolution, bone strain, bone stress, safety factor.

INTRODUCTION

Recent studies of limb bone loading during the terrestrial locomotion of reptilian and amphibian taxa (Blob and Biewener, 1999; Blob and Biewener, 2001; Butcher and Blob, 2008a; Butcher et al., 2008; Sheffield and Blob, 2011) have identified several distinctions between the patterns typical of these groups and those found in previously studied species of birds and mammals (Rubin and Lanyon, 1982; Biewener, 1983a; Biewener et al., 1988; Carrano, 1998; Demes et al., 2001; Lieberman et al., 2004; Main and Biewener, 2004; Main and Biewener, 2007). Reptiles and amphibians that make use of sprawling limb postures tend to show more prominent limb bone torsion than quadrupedal mammals, but also higher limb bone safety factors than birds or mammals. In a further contrast among these groups, avian and mammalian limb bones have generally similar mechanical properties and resistance to failure (Alexander, 1981; Biewener, 1982; Biewener, 1993; Erickson et al., 2002), whereas the elevated safety factors of amphibians and reptiles may be related to low magnitude loading, high resistance to failure or a combination of both, depending on the taxon (Sheffield and Blob, 2011).

The broad similarities of limb bone loading mechanics among amphibian and reptilian species might be related to a number of factors. For example, high safety factors in these groups may be adaptations that serve as insurance against widely variable loads (Lowell, 1985) or slow rates of bone repair (de Ricqlès, 1975; de Ricqlès et al., 1991). The patterns of limb bone loading mechanics seen in amphibians and non-avian reptiles may also represent retained ancestral traits, from which birds and mammals diverged independently (Blob and Biewener, 1999; Blob and Biewener, 2001; Butcher and Blob, 2008a; Sheffield and Blob, 2011). Though plausible based on available data, such a conclusion would be based on a limited sample of four taxa among amphibian and reptilian species. Among non-avian reptiles, lizards are one of the most diverse groups, with a wide range of habits and locomotor performance capacities (Irschick and Jayne, 1999). Sampling a lizard species from a different lineage than that previously examined, particularly one with locomotor habits that differ from the rapid running shown by the sub-adult iguanas previously tested (Blob and Biewener, 1999; Blob and Biewener, 2001) could help to determine whether bone loading patterns are

similar across the breadth of the group and distinct, as a whole, from those of birds and mammals.

To clarify whether the limb bone loading patterns observed in iguanas, crocodilians and turtles are representative of non-avian reptiles, we evaluated the loading mechanics of the femur in Argentine black and white tegus, *Tupinambis merianae* (Duméril and Bibron 1839), during terrestrial walking using force-platform analysis (Biewener and Full, 1992) and implanted strain gauges (Biewener, 1992). We also compared load magnitudes with bone mechanical property data from tegus to calculate limb bone safety factors. Tegus are members of the family Teiidae in the scleroglossan clade and, thus, are phylogenetically distant from previously studied *Iguana iguana* (Blob and Biewener, 1999; Blob and Biewener, 2001) in the iguanian clade (Estes et al., 1988; Macey et al., 1997). *Tupinambis merianae* also have different locomotor habits than iguanas: whereas iguanas are herbivores that tend to flee as prey until reaching very large size, tegus are active carnivorous foragers that, though capable of rare bursts of speed, tend to walk slowly as they survey their environment for olfactory cues with their tongue (Gudynas, 1981). Tegus thus provide a particularly interesting taxon for comparison with salamanders, which are also typically slow walkers (Ashley-Ross, 1994; Reilly et al., 2006). Our study of limb bone loading in tegus will therefore allow us to test the hypothesis that low limb bone loads, high safety factors and prominent limb bone torsion are characteristic patterns in lizards and in sprawling ectothermic tetrapods more generally, helping to clarify understanding of the evolution of tetrapod locomotor mechanics and skeletal design.

MATERIALS AND METHODS

Animals

Five Argentine black and white tegu lizards were used in experiments: three juveniles (0.11–0.17 kg body mass) used for force-platform analyses and two adults (one male and one female, 2.72–4.55 kg body mass) used in our *in vivo* strain analyses. Tegus were purchased from Glades Herp (Bushnell, FL, USA), MB Reptiles (Grants Pass, OR, USA) and LLL Reptile (Oceanside, CA, USA). After initiation of the study, sample sizes of individuals (particularly large lizards) were limited by availability of animals for purchase. Tegus are large, primarily carnivorous teiid lizards from South America that are active foragers and can be found in a variety of habitats, including rocky outcroppings and the forest floor (Gudynas, 1981). They walk using a sprawling posture and generally hold their entire weight off the ground during locomotion (Urban, 1965). All lizards were kept in a greenhouse and exposed to ambient light conditions; daytime temperatures were typically 30°C, and nighttime temperatures were kept above 25°C using ceramic heat lamps with automatic on–off sensors. Adult lizards were kept in large plastic tubs (1.6×1.3×0.4 m length×width×height) lined with cedar bedding, and juveniles were kept in 20 gallon glass terraria filled with reptile bedding; all enclosures provided shaded areas. Tegus were given fresh water and fed canned dog food or crickets every day. For approximately 2 to 4 weeks prior to experiments, lizards were trained to walk on a motorized treadmill (model DC5; Jog A Dog®, Ottawa Lake, MI, USA), which involved 5–10 min bouts of walking at moderate speed several times weekly. All experimental procedures followed Clemson University IACUC approved guidelines and protocols (AUP ARC2007-029). After the completion of experimental data collection, tegus were euthanized by overdose of pentobarbital sodium solution (Euthasol®, Delmarva Laboratories Inc., Midlothian, VA, USA; 200 mg kg^{-1} intraperitoneal injection) and frozen for later dissection and measurement of anatomical variables and limb bone mechanical properties.

Data collection: three-dimensional kinematics and ground reaction forces

Because of the behavioral recalcitrance of the adult tegus, force-platform data were collected only from the three juvenile animals. Juvenile tegus were filmed simultaneously in lateral and dorsal views at 200 Hz using two synchronized high-speed digital video cameras (Phantom v.4.1, Vision Research Inc., Wayne, NJ, USA) as they walked across a custom-built force platform (K&N Scientific, Guilford, VT, USA) that was inserted into a wooden trackway [for details see Butcher and Blob (Butcher and Blob, 2008a)]. The platform and trackway were configured as in our previous study of salamanders (Sheffield and Blob, 2011), except that a larger surface of the platform was exposed (10×11 cm), and the wood of the trackway was covered with textured paint (rather than surgical drape) to ensure traction.

Lizards were encouraged to walk by gently squeezing the base of each animal's tail and by enticing them with a cricket taped onto the end of a wooden dowel. Animals were allowed to choose their own walking speed during trials. Successful trials consisted of filming a complete isolated footfall of the right hindlimb on the plate with as little overlapping contact on the plate from the right forelimb as possible. Temperature in the trackway was maintained at 20–21.5°C, with trial sessions lasting for 1 h before tegus were returned to their enclosure.

Procedures for digitizing and processing video data on limb position closely followed those used in our study of femoral loading in salamanders (Sheffield and Blob, 2011), producing smoothed kinematic data normalized to the same duration (101 points) for all trials. Specifications of our force platform, amplifiers and data acquisition system were reported previously (Butcher and Blob, 2008a; Sheffield and Blob, 2011). Force data were collected at 5000 Hz and amplifier gains were adjusted appropriately for the body mass of the lizards to maximize the sensitivity of ground reaction force (GRF) resolution. Procedures for force calibration, smoothing and synchronization of force data with video, and evaluation of the point of application of the GRF, were performed following protocols used in our previous studies (Butcher and Blob, 2008a; Sheffield and Blob, 2011).

Steps of the right hindlimb (N=15–18 per animal) were selected for analysis. Qualitative criteria for selection of runs included minimization of overlapping forelimb contact on the force platform, straightness of motion across the plate and continuity of locomotor speed. As for salamanders (Sheffield and Blob, 2011), animal speed for each trial was calculated (m s^{-1}) by differentiating the cumulative displacement of a body landmark and then normalizing speeds by body length (BL s^{-1}) for comparisons among individuals. After synchronizing force and kinematic data, GRF components and joint moments were calculated to allow evaluation of femoral stresses (Sheffield and Blob, 2011). Inertial and gravitational moments about the hindlimb joints were assumed to be negligible during stance (Alexander, 1974; Biewener and Full, 1992).

Bone stress analyses

As in our analyses of femoral stresses in salamanders, forces acting on tegu hindlimbs were resolved into a frame of reference defined by the anatomical planes of the limb segments following standard designations for sprawling animals [see fig. 1 in Blob and Biewener (Blob and Biewener, 2001)]. Calculations and equations for bone stress analyses closely followed those previously published for

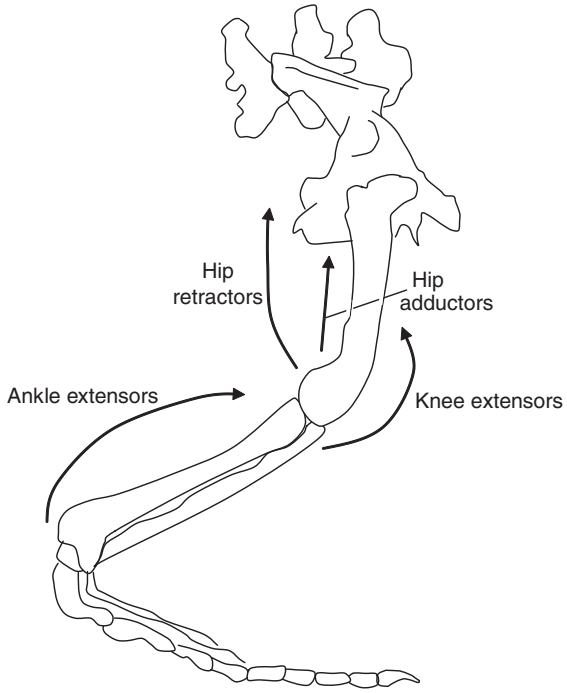

Fig. 1. Outline (right lateral view) of the hindlimb skeleton of *Tupinambis merianae* illustrating the lines of action of the major muscle groups contributing to stresses in the femur during the stance phase of terrestrial locomotion. Rotational forces exerted by the caudofemoralis muscle (limb retractor) were not calculated (Materials and methods).

iguanas and alligators (Blob and Biewener, 2001) and river cooter turtles (Butcher and Blob, 2008a) and are not repeated here. Briefly, femoral stresses were calculated at mid-shaft (Biewener and Taylor, 1986), so that only the GRF and forces exerted by muscles spanning the mid-shaft of the femur entered directly into calculations of peak bending stress (Fig. 1, Table 1). When multiple muscles were active to counteract the GRF moment at a joint, a weighted mean moment arm was calculated for the group based on the physiological cross-sectional areas (PCSA) of each muscle (Alexander, 1974). Muscle moment arms were measured during specimen dissections with the limbs held in a midstance position; PCSAs (Table 1) were calculated following published protocols (Biewener and Full, 1992).

Our model of muscle forces placing stress on the femur was adapted from one previously published for lizards (Blob and Biewener, 2001) and included extensors of the ankle, flexors and extensors of the knee, and femoral adductors and retractors (Fig. 1) [see appendices in Blob and Biewener (Blob and Biewener, 2001), Butcher and Blob (Butcher and Blob, 2008a) and Sheffield and Blob (Sheffield and Blob, 2011)]. Key model features include the following characteristics. First, muscles are assumed to act in the same anatomical plane throughout stance. Second, seven muscles [adductor femoris, pubotibialis, flexor tibialis externus, flexor tibialis internus (FTI), flexor tibialis internus 2 deep (FTI2d), flexor tibialis internus 2 superficial (FTI2s) and puboishiotibialis] are in positions to contribute to adductor moments at the hip. All of these muscles span the femoral mid-shaft, countering the abductor moment of the GRF at the hip and bending the femur to place its ventral cortex in compression. Although the GRF protractor moment would be countered by the caudofemoralis longus (CFL) as a retractor, primary attachment of the CFL is proximal to mid-shaft, so it does not contribute to calculations of mid-shaft stress (Blob and Biewener, 2001). Third, knee extensors (femorotibialis and iliotibialis) on the dorsal surface of the femur counter the combined knee flexor moments of the GRF, femoral adductors and ankle extensors (peroneus, flexor digitorum longus, and the medial and lateral gastrocnemius) that span the knee (Table 1). The bending moment induced by the knee extensors opposes that induced by hip adductors, placing the dorsal femoral cortex in compression. Because muscles crossing the hip and knee have opposing actions, there is no unique solution to muscle force calculations; however, the model we apply in this study accounts for known co-activation of antagonist muscle groups to the extent possible (Blob and Biewener, 2001). Fourth, muscular contributions to femoral torsion (i.e. shear stresses) were not estimated because of uncertainty about the activity of antagonist femoral rotators; instead, shear stress induced by the GRF alone was calculated as a minimum estimate of torsion (Blob and Biewener, 2001; Butcher and Blob, 2008a).

Table 1. Anatomical data from hindlimb muscles of experimental animals (*Tupinambis merianae*)

	tm04			tm05			tm06		
Muscle	*A*	θ	r_m	*A*	θ	r_m	*A*	θ	r_m
Hip adductors									
Puboischiotibialis	4.7	10	2.9^h	8.1	15	2.4^h	3.5	15	1.2^h
FTI	7.6	12	3.7^h	5.7	15	4.7^h	4.9	15	3.4^h
FTI2s	2.2	10	3.7^h	3.6	15	5.1^h	1.8	15	3.0^h
FTI2d	4.5	10	10.0^h	6.2	15	6.3^h	7.2	10	5.1^h
FTE	7.9	10	7.5^h	8.3	10	7.1^h	4.2	10	3.5^h
Pubotibialis	1.8	12	3.4^h	2.0	13	2.2^h	4.1	10	6.2^h
Adductor femoris	4.7	10	4.0^h	5.1	10	4.3^h	3.3	10	3.0^h
Knee extensors									
Iliotibialis	8.6	13	3.6^h, 2.5^k	1.1	15	4.0^h, 3.7^k	2.3	14	2.6^h, 2.8^k
Femorotibialis	6.4	26	1.7^k	9.9	25	1.5^k	4.9	23	2.2^k
Ankle extensors									
L. gastrocnemius	11.1	26	3.0^k, 2.9^a	4.6	30	3.3^k, 2.4^a	31.0	28	2.6^k, 3.1^a
M. gastrocnemius	6.4	30	4.6^k, 1.9^a	20.6	22	2.6^k, 3.3^a	18.9	22	1.8^k, 3.1^a
FDL	5.7	12	1.6^k, 4.5^a	9.5	15	1.6^k, 1.9^a	7.8	13	1.7^k, 1.8^a
Peroneus longus	3.2	0	1.4^k, 1.1^a	4.4	0	1.7^k, 1.2^a	2.6	0	1.1^k, 1.2^a

Individual animals are identified by alphanumeric codes in the column headings (e.g. tm04).

A, cross-sectional area of muscle (mm^2); FDL, flexor digitorum longus; FTE, flexor tibialis externus; FTI, flexor tibialis internus; r_m, moment arm of the muscle (mm) about the joint indicated by the superscript letter (a, ankle; h, hip; k, knee); θ, angle between the muscle and the long axis of the femur (deg); L, lateral; M, medial.

Table 2. Anatomical data from femora of experimental animals (*T. merianae*)

Measurement	tm04	tm05	tm06
Length (mm)	29.87	31.25	27.07
A (mm^2)	2.24	2.68	2.52
$r_{c(AP)}$ (mm)	0.64	0.13	0.29
$r_{c(DV)}$ (mm)	–0.52	–0.27	–0.30
$y_{(AP)}$ (mm)	1.26	1.47	1.24
$y_{(DV)}$ (mm)	1.38	1.51	1.29
I_{AP} (mm^4)	2.00	2.85	2.00
I_{DV} (mm^4)	1.98	2.77	2.05
J (mm^4)	3.98	5.62	4.05

Individual animals are identified as in Table 1.

A, cross-sectional area of bone; *I*, second moment of area; *J*, polar moment of area; r_c, moment arm due to bone curvature; *y*, distance from neutral axis to cortex.

In subscript notations, AP denotes the anatomical anteroposterior direction for the femur, and DV denotes the anatomical dorsoventral direction for the femur.

Curvature sign conventions: AP, +=concave posterior, –=concave anterior; DV, +=concave ventral, –=concave dorsal.

After calculating estimates of muscle forces, bending moments and axial and bending stresses for the femur were calculated following the methods we applied for three-dimensional analyses in salamanders (Sheffield and Blob, 2011). Measurements of skeletal variables (Table 2) were determined from digital photographs (Sheffield and Blob, 2011) using a custom analysis macro for NIH Image to calculate cross-sectional variables (Lieberman et al., 2003). Bending moments and stresses were calculated in the perpendicular dorsoventral (DV) and anteroposterior (AP) directions (Blob and Biewener, 2001), and accounted for bending induced by axial forces due to the moment arm of bone curvature, r_c (Biewener 1983a; Biewener, 1983b). Calculations for the orientation of peak bending stress and torsional stress (τ) caused by the GRF followed published methods (Blob and Biewener, 2001; Butcher and Blob, 2008a; Sheffield and Blob, 2011).

Strain analyses: surgical implantation procedures

Only adult tegus were sufficiently large to allow the implantation of gauges for the measurement of femoral strains. Strain gauges were attached surgically to the right femur of two animals using aseptic technique and following published methods (Biewener, 1992; Blob and Biewener, 1999; Butcher et al., 2008). All surgical and experimental procedures followed protocols approved by the Clemson University IACUC (AUP ARC-2007-029). Initial doses of 1 mg kg^{-1} butorphenol and 50 mg kg^{-1} ketamine were injected into the forelimb musculature to induce analgesia and a surgical plane of anesthesia, with supplemental doses administered as required.

To expose strain gauge attachment sites, longitudinal incisions were made through the skin on the anteroventral aspect of the thigh at mid-shaft. Muscles surrounding the femur were separated along the fascial plane between the ambiens and the pubotibialis, which were retracted to gain access to the bone. Gauges were attached at mid-shaft *via* this single incision. At the site where gauges were to be attached, a 'window' of periosteum was removed to expose the bone cortex. Bone surfaces were gently scraped with a periosteal elevator, swabbed clean with ether using a cotton-tipped applicator and allowed to dry for several seconds. Gauges were then attached using a self-catalyzing cyanoacrylate adhesive (Duro^{TM} Superglue, Henkel Loctite Corp., Avon, OH, USA).

Single element (SE) and rosette (ROS) strain gauges (type FLG-1-11 and FRA-1-11, respectively; Tokyo Sokki Kenkyujo, Japan) were attached to surfaces of the femur and given relative anatomical designations of 'dorsal,' 'anterodorsal' and 'anterior', following conventions of anatomical orientation established for reptiles (Blob and Biewener, 2001; Butcher and Blob, 2008a). Precise anatomical locations were determined from sections of the bones after the completion of the experiments (see below). Only one ROS gauge was used in each individual and was attached at the 'anterior' location in both. SE gauges were attached to the other bone surfaces after placement of the ROS. SE and central elements of ROS were aligned (within 5 deg) with the long axis of the femur. Once all gauges were in place, lead wires from the gauges (336 FTE, etched Teflon; Measurements Group, Raleigh, NC, USA) were passed subcutaneously though a small, proximal skin incision on the anterodorsal aspect of the upper thigh, after which all incisions were sutured closed. Lead wires were then soldered into a microconnector and solder connections were reinforced with epoxy adhesive. Exposed portions of the lead wires were wrapped in self-adhesive bandage to form a protective cable. The microconnector then was secured (with slack) to the dorsal side of the animal's right hip by attaching the lead wire cable to a self-adhesive bandage that was wrapped around the body.

In vivo strain data collection and data analyses

After 1–3 days of recovery, *in vivo* strain recordings were made over the subsequent 2 days. Strain signals were conducted from the gauges to Vishay conditioning bridge amplifiers (model 2120B; Measurements Group) *via* a shielded cable. Raw voltage signals from strain gauges were sampled through an A/D converter (model PCI-6031E; National Instruments) at 5000 Hz, saved to computer using data acquisition software written in LabVIEW^{TM} (v. 6.1; National Instruments) and calibrated to microstrain ($\mu\varepsilon$). Strain data were collected while animals walked on the motorized treadmill used for locomotor training. Most recordings consisted of short trials of moderate (0.1–0.3 BL s^{-1}), steady-speed walking with data sampled from two to six consecutive footfalls of the right hindlimb. Periods of rest were given between trials, and temperature within the treadmill enclosure was maintained near or above 25°C by heat lamps for all trials.

To document locomotor behavior and footfall patterns during strain trials, lateral and posterior view high-speed (100 Hz) video data (Phantom v. 4.1; Vision Research Inc.) of locomotion were collected. Videos were synchronized with strain recordings as described for force-platform analyses (Butcher and Blob, 2008a; Sheffield and Blob, 2011). Upon completion of strain recordings, animals were euthanized by an overdose of a pentobarbital sodium solution (Euthasol®; 200 mg kg^{-1} intraperitoneal injection) and frozen for later dissection, verification of gauge placement and limb bone mechanical property tests.

Standard conventions for analysis and interpretation of strain data were employed, following our previous studies of non-avian reptile limb bone loading (Blob and Biewener, 1999; Butcher et al., 2008). Briefly, tensile strains are recorded as positive and compressive strains as negative. The magnitudes of peak axial strains (aligned with the long axis of the femur) were determined from each gauge location for each step of the right hindlimb. Strain magnitudes were evaluated for 12–34 steps from each lizard (depending on the quality of recordings from each individual), with raw strains zeroed during swing phase prior to each consecutive footfall. Magnitudes and orientations of peak principal strains (i.e. maximum and minimum strains at each site, regardless of alignment with the femoral long axis), as well as

shear strain magnitudes, were calculated from ROS data following published methods (Carter, 1978; Dally and Riley, 1978; Biewener and Dial, 1995), allowing evaluation of the importance of torsional loading in tegu femora. Defining the long axis of the femur as 0 deg, pure torsional loads would show principal strain orientations (deviations from the bone long axis) of 45 or –45 deg, depending on whether the femur was twisted in a clockwise or counterclockwise direction, respectively. Orientations of principal tensile strain (ϕ_t) differing by 180 deg are equivalent, and orientations of peak principal tensile and compressive strains are orthogonal.

Following muscular dissections of the hindlimbs of the animals, instrumented femora were excised, swabbed clean of tissue and embedded in fiberglass resin. Transverse sections were cut from each embedded femur through the mid-shaft gauge locations, and one cross-section from each femur was then photographed using a digital camera mounted on a dissecting microscope. Microsoft PowerPoint was used to trace outlines of the cross-sections from the photographs, mark locations of the three gauges on the bone perimeter and save cross-sectional tracings as JPEG files. Each bone's geometric data were then input along with strain data from its three femoral gauge locations into analysis macros for the public domain software NIH Image for Macintosh (http://rsb.info.nih.gov/nih-image/) in order to calculate the location of the neutral axis (NA) of bending and the planar distribution of longitudinal strains through femoral cross-sections (Lieberman et al., 2003; Lieberman et al., 2004). The distribution of tensile and compressive strains on the cortex of the femur then was used to evaluate the loading regime the bone experienced during locomotion. For instance, equal magnitudes of tensile and compressive strain on opposite cortices would indicate pure bending, whereas unequal magnitudes of tension and compression at different cortical locations would indicate a combination of axial and bending loads. Planar strain analyses were conducted on a subset of data (N=10 steps; one individual), allowing calculation of peak values of tensile and compressive strain that may have occurred at locations other than recording sites (Carter et al., 1981; Biewener and Dial, 1995). Calculated peak strains were then compared with measured peak strains to determine the proportional increase in strain between the recorded peaks and calculated peak magnitudes. Additionally, in a subset of these data (N=5 steps), planar strain distributions were calculated at five time points during a step (15, 30, 50, 70 and 85% contact) (Butcher et al., 2008) to evaluate shifts in the location and orientation of the NA throughout the step.

Mechanical properties tests and safety factors

Because of the small size of the juvenile tegu femora, yield stress and strain in bending were determined from the femora (N=6) using microindentation tests following procedures previously described for salamanders (Sheffield and Blob, 2011). Values of Vickers hardness (H_V) for each specimen were entered into linear regression equations (Wilson et al., 2009) based on published data (Hodgskinson et al., 1989) from cortical bone specimens of four taxa from diverse lineages that allowed calculation of tensile yield stress (σ_y) and strain (ε_y):

$$\sigma_y = 32.571 + 2.702\overline{H}_V, \quad (1)$$

$$\varepsilon_y = 0.011 - 6.537\times10^{-5}\,(\overline{H}_V). \quad (2)$$

As noted for our analyses of salamanders (Sheffield and Blob, 2011), estimates of tensile yield stress and strain based on converted values of hardness may incur error, but the high R^2 values of the regressions that we employed (Wilson et al., 2009) indicates that such error was minimized to the extent possible. Safety factors for *T. merianae* femora in bending were calculated as the ratios of tensile yield stress and strain to peak tensile locomotor stress and strain, respectively, with 'mean' and 'worst-case' estimates calculated as in our previous studies (Blob and Biewener, 2001; Butcher and Blob, 2008a; Sheffield and Blob, 2011).

Failure strains were evaluated in torsion (model 8874 biaxial testing machine with 25 kN load cell; Instron, Norwood, MA, USA) for whole bone specimens (N=4 femora; N=5 tibiae, including bones from a third individual) of adult tegus that were not instrumented during *in vivo* strain recording trials. Limited previous data have not indicated significant differences in limb bone mechanical properties between juvenile and adult lizards (Peterson and Zernicke, 1987). Procedures followed those described previously for turtle femora tested in torsion (Butcher and Blob, 2008a; Butcher et al., 2008). Briefly, two ROS gauges were attached to the mid-shaft of each bone (femur: dorsal and ventral surfaces; tibia: anterior and posterior surfaces). Strain gauge signals were amplified, sampled (1000 Hz) through an A/D converter in LabVIEW, and calibrated as detailed previously. Bones were suspended in machined aluminum wells into which epoxy was poured to embed ~15 mm of the ends of each bone. Once hardened, embedded ends were fitted into mounting brackets in the testing jig and twisted to failure. Applied load and displacement data were sampled at 10 Hz until failure. Twisting rate was set at 3 deg s^{-1} (Furman and Saha, 2000) and performed in a direction to simulate *in vivo* anterior (i.e. inward) rotation. Failure point was identified from linear plots of applied twisting moment (torque, T) *versus* maximum shear strain. Torsional stress (τ) at failure was calculated as:

$$\tau = T\,(y_t / J), \quad (3)$$

where y_t is the distance from the centroid of the bone to the cortical surface and J is the polar moment of area (Wainwright et al., 1976). A strain-based safety factor in shear for the femur of *T. merianae* was calculated as the ratio of failure strain to peak locomotor shear strain. The 'mean' safety factor in shear was calculated from the mean value of peak locomotor shear strain multiplied by a proportional value of strain increase determined from planar strain analyses (Blob and Biewener, 1999; Butcher et al., 2008). Application of the planar strain correction factor to shear strains requires an assumption that shear strains increase in proportion to normal strains around a bone cortex. Although this assumption is an oversimplification, it helps to account for variation in shear strains around the limb bone cortex, as indicated in studies of alligators from which simultaneous recordings were obtained from two ROS gauges [e.g. differing by a factor of 1.7 at 0.4 BL s^{-1} (Blob and Biewener, 1999)]. Thus, this assumption prevents underestimation of shear strains that would artificially inflate safety factor estimates. As reptiles have been hypothesized to have high limb bone safety factors, our assumption is more conservative for the questions we are addressing than calculation of safety factors from uncorrected shear strains, which would involve an alternate simplifying assumption that the femur is a perfect cylinder loaded in pure torsion and has equal shear strains around its entire circumference.

RESULTS

Overview of stance-phase kinematics

At the beginning of stance, the femur is slightly abducted and positioned so that it is almost parallel to the ground (mean ± s.e.m.=9±2 deg, relative to a horizontal plane at 0 deg; Fig. 2). The femur is also in a protracted position at the beginning of stance (38±2 deg, relative to a 0 deg axis perpendicular to the body),

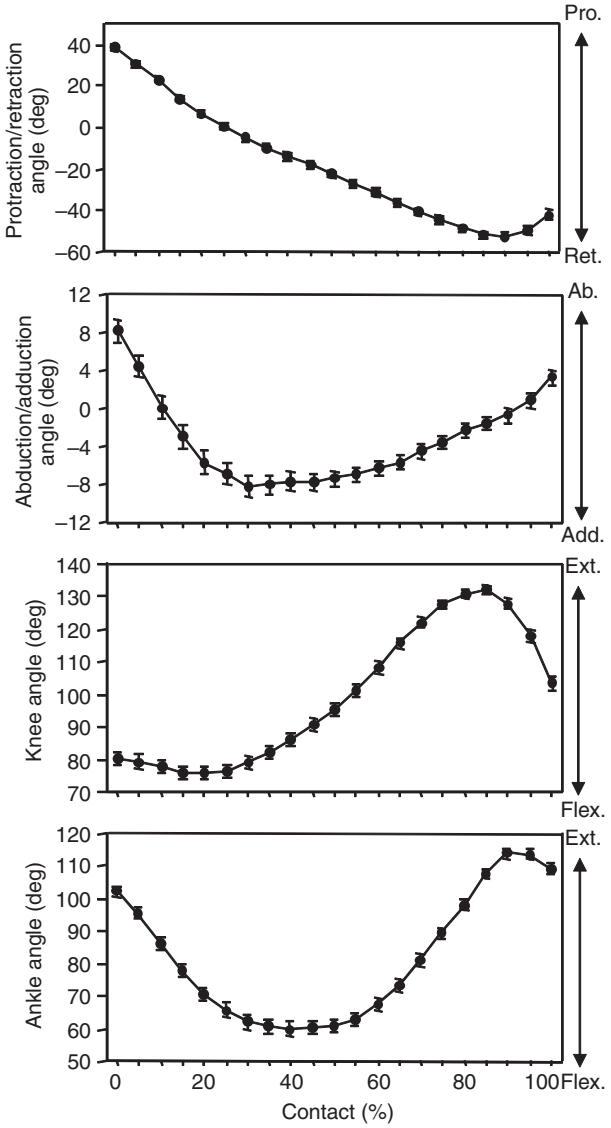

Fig. 2. Representative kinematic profiles of right hindlimb joints for tegus (*T. merianae*) during a walking step over a force platform. Top to bottom: femoral (hip) protraction (Pro.)/retraction (Ret.) angle, femoral (hip) abduction (Ab.)/adduction (Add.) angle, knee angle and ankle angle (Ext., extension; Flex., flexion). Kinematic profiles represent mean (±s.e.m.) angles averaged across all three tegus (*N*=15–18 trials per individual, 49 total steps per data point). Note that *y*-axis scales differ for these plots to provide increased resolution for smaller angles.

whereas the tibia is positioned so that the knee is anterior and lateral to the ankle. Foot posture is plantigrade, and the digits point forward and slightly laterally. During stance, the femur retracts through a range of almost 95 deg. It is adducted by approximately 20 deg through the horizontal plane by midstance before abducting back to a nearly horizontal position by the end of stance (Fig. 2). The knee extends through a range of almost 70 deg before flexing by nearly 25 deg by the end of stance. The ankle begins stance by flexing to accommodate the weight of the body, but then extends as the tegu pushes off the substrate (Fig. 2), causing the tibia to approach a nearly horizontal AP orientation parallel to the ground at the end of the step.

GRF magnitude and orientation

Speeds of juvenile tegus averaged 0.9±0.2 BL s^{-1}, with one individual typically faster than the other two (Table 3). Video records from our trials indicated that overlap of the right hindlimb with the right forelimb during force plate contact averaged 19.8±1.2% across all trials. Although substantial, this overlap ends well before midstance, where limb bone loading was highest in previous published data from iguanas (Blob and Biewener, 2001). Moreover, comparison of the timing of peak GRF between steps with overlap (*N*=45) and steps with no overlap (*N*=4) indicated only a 6% difference, with both groups showing mean peak GRF times (30 and 36% of stance, respectively) well after the mean period of overlap. Any runs showing peak GRF during forefoot overlap (or up to 2% of step duration after forefoot overlap) were excluded, and our discussion of GRF orientation and magnitude focuses only on the portion of the step through which the hindlimb is in isolated contact with the force plate. Peaks appearing in figures prior to the end of overlap are artifacts of the combined force of two limbs on the force platform at once, and should not be interpreted as actual peak forces or stresses for the hindlimb.

The GRF is oriented upward, medially and anteriorly throughout almost all of stance phase, with the vertical component substantially larger in magnitude than both the anteroposterior and mediolateral components (Fig. 3). The net GRF reaches peak magnitude almost one-third of the way through the contact interval (pooled mean: 30.8±1.8% contact; Table 3). Peak net GRF magnitude averaged 0.47±0.02 BW across all three tegus (0.59±0.05 BW for tm04, the individual showing the highest forces), with an essentially vertical orientation through the middle 20–60% of the contact interval (pooled mean at peak net GRF: AP angle, 8.4±1.8 deg; ML angle, –14.4±1.1 deg; vertical=0 deg in both directions with positive values indicating anterior and lateral inclinations; Table 3; Fig. 3B,C). The net GRF vector is also directed almost perpendicular to the femur for most of the step, increasing to a mean of 111.3±1.6 deg relative to the femur across all three tegus at peak net GRF magnitude (Fig. 3; Table 3). With the near-vertical orientation of the GRF, rotation of the femur about its long axis (counterclockwise when viewing the right femur from its proximal end) would contribute to shifting the axis of femoral bending from DV (i.e. about a neutral axis close to the anatomical AP axis) towards AP (i.e. about a neutral axis close the anatomical DV axis).

Moments of the GRF about hindlimb joints

The GRF exerts moments in a consistent direction through most of stance for most hindlimb joints. Because the GRF originates anterior to the ankle, it tends to dorsiflex the ankle for nearly all of stance phase, although this dorsiflexion moment does decrease in magnitude through most of the contact interval (Fig. 4). Ankle extensor muscles would need to be active to counter this moment. The GRF exerts a flexor moment at the knee for the beginning of stance, but this moment is small during isolated contact of the hindlimb with the force platform, and changes orientation to briefly reach an extensor peak at approximately 30% of contact, followed by another change and a flexor peak at approximately 75% of contact (Fig. 4). The upward orientation of the GRF also gives a consistent abductor moment at the hip that reaches an early peak and subsequently decreases to zero (Fig. 4). To maintain equilibrium, this moment would require activity by femoral adductors. The GRF also induces a protractor moment for all of stance, which reaches a peak at approximately 70% of the contact interval (Fig. 4).

The GRF exerts torsional moments that would tend to rotate the right femur clockwise (i.e. outward), viewing it from its proximal

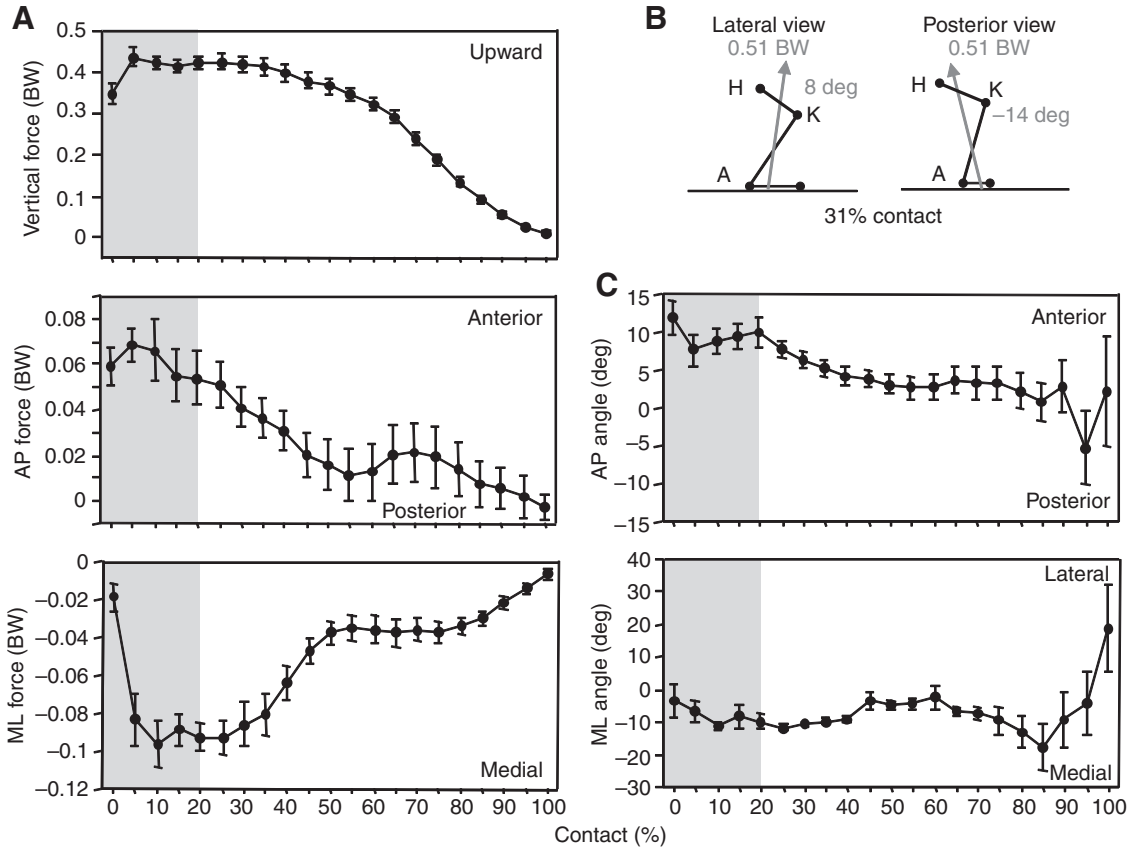

Fig. 3. Mean ground reaction force (GRF) dynamics for the right hindlimb of tegus. All plots show means (±s.e.m.) averaged across all three tegus (N=15–18 trials per individual, 49 total steps per data point). (A) Vertical, anteroposterior (AP) and mediolateral (ML) GRF components in body weights (BW), with positive values indicating upward, anterior and lateral forces, respectively (top to bottom). *Y*-axis scales differ for these plots to provide increased resolution for the small AP and ML forces. All trials were normalized to the same duration, allowing values to be graphed against the percentage of time (contact) through the stance phase. (B) Limb segment positions at the mean time of peak net GRF (31% contact) during a representative step by *T. merianae*, with the direction and magnitude of the GRF vector illustrated. The femur is highlighted by bolder lines; note that it is foreshortened in lateral view. H, hip; K, knee; A, ankle. (C) AP and ML orientations of the net GRF vector. AP angles were determined relative to vertical at 0 deg (90 deg indicates GRF horizontal, pointing forward; <0 deg indicates posteriorly directed GRF). ML angles were determined relative to vertical at 0 deg (negative values indicate medially directed GRF). Grey shading over initial 20% of traces in A and C indicates the mean period of forelimb overlap with hindlimb contact across individuals.

end (Fig. 4). As the hip moves forward and the femur retracts, torsional moments increase to a maximum approximately halfway through the contact interval. After this maximum, the torsional moment decreases until approximately 70% of contact, at which point the magnitude of the rotational moment on the femur remains small but stable (Fig. 4).

Femoral stresses

Bending stresses induced by the axial component of the GRF are small and have little impact on limb loading patterns (Fig. 5). In contrast, hindlimb muscles appear to make substantial contributions to bending stresses in the femur because of the large moments exerted by the GRF in the abductor direction at the hip that these

Table 3. Mean peak ground reaction force (GRF) data for *T. merianae*

	GRF								
Individual	Vertical (BW)	AP (BW)	Peak net ML (BW)	GRF time (%)	Net GRF (BW)	GRF femur angle (deg)	GRF AP angle (deg)	GRF ML angle (deg)	Speed (BL s^{-1})
tm04 (N=18)	0.59±0.05	0.05±0.03	–0.21±0.05	27.2±2.6	0.64±0.07	111.9±2.5	5.8±1.9	–16.7±1.8	1.6±0.47
tm05 (N=16)	0.42±0.04	0.05±0.01	–0.08±0.01	33.0±2.4	0.43±0.01	106.1±1.6	6.2±1.0	–10.8±1.0	0.4±0.05
tm06 (N=15)	0.39±0.03	0.11±0.04	–0.10±0.01	32.9±4.2	0.45±0.09	116.2±3.7	14.1±5.2	–15.4±2.4	0.6±0.04
Mean	0.47±0.02	0.07±0.02	–0.13±0.02	30.8±1.8	0.51±0.03	111.3±1.6	8.4±1.8	–14.4±1.1	0.9±0.19

BW, body weight; BL, body length; GRF AP angle, anteroposterior inclination angle of GRF; GRF femur angle, angle of GRF to the femur; GRF ML angle, mediolateral inclination angle of GRF.
Vertical=0 deg for GRF AP and ML angles of inclination; for GRF AP, positive angles are anteriorly directed; for GRF ML, negative angles are medially directed.
Values are means ± s.e.m.; N, number of steps analyzed.

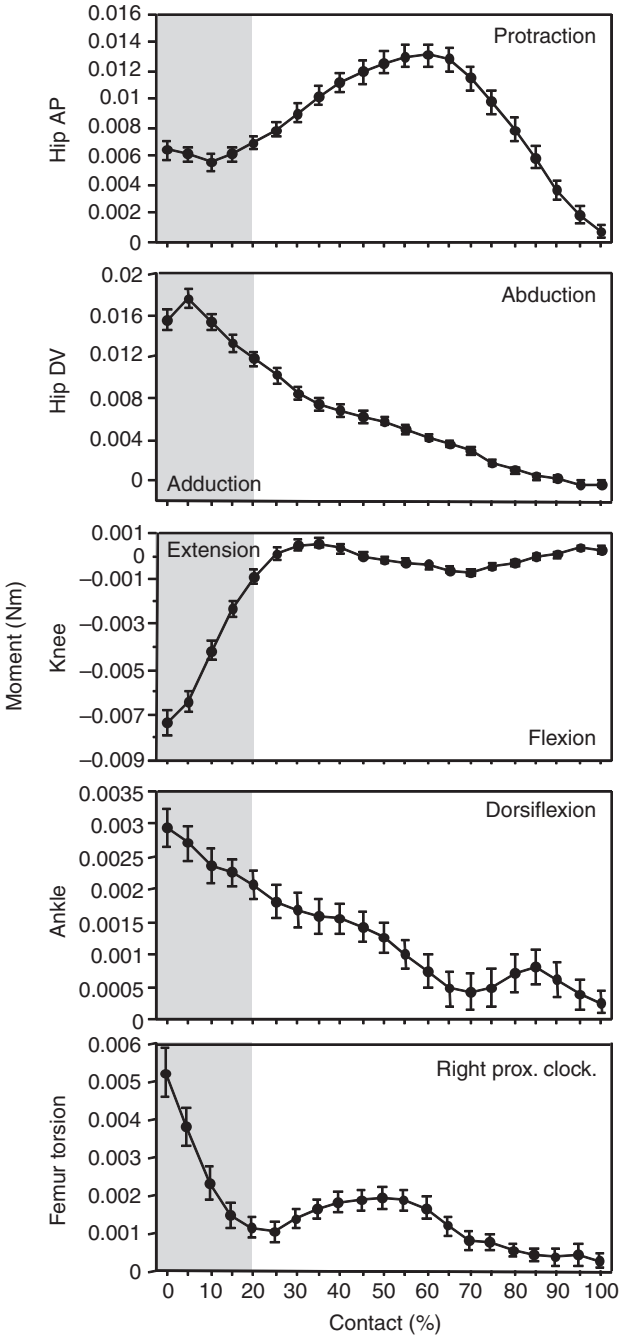

Fig. 4. Moments exerted by the GRF about the hindlimb joints and the long axis of the femur during walking steps in tegus. All plots show means (±s.e.m.) averaged across all three tegus (N=15–18 trials per individual, 49 total steps per data point). Note that y-axis scales differ for these plots to provide greater resolution for smaller moments. Directions of moments are labeled to the right of the figure plots. Hip AP, the GRF moment about the hip in the anatomical anterior and posterior directions acting to protract or retract the femur; Hip DV, the GRF moment about the hip in the anatomical dorsal and ventral directions acting to abduct or adduct the femur; Right prox. clock., torsional GRF moment, clockwise when viewing the right femur from the proximal end. Grey shading over initial 20% of traces indicates the mean period of forelimb overlap with hindlimb contact across individuals.

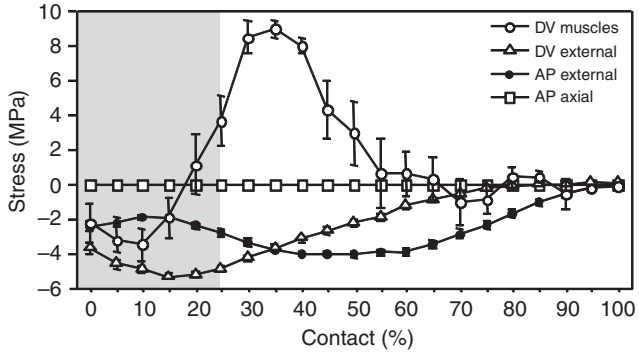

Fig. 5. Components of bending stress in the femur induced by muscles and GRF components from an individual tegu. All data are mean (±s.e.m.) stresses over N=16 trials. Stresses plotted are those occurring on the dorsal surface for forces acting to cause dorsoventral (DV) bending, and those occurring on the anterior surface for forces acting to cause anteroposterior (AP) bending. Tensile stress is positive and compressive stress is negative. 'Muscles' indicates stresses induced by major muscle groups in the direction indicated; 'external' indicates stresses induced by the GRF acting in the direction indicated; 'axial' indicates stresses induced by the axial component of the GRF due to bone curvature in the direction indicated. Bending stresses induced by axial forces are very small and overlap along the zero line for the AP directions. Grey shading over initial 20% of traces indicates the period of forelimb overlap with hindlimb contact.

muscles must counter (Fig. 5). In the DV direction, contraction of the adductor muscles bends the femur in the opposite direction from the knee extensors and the external action of the GRF. Because the adductors must exert such large forces to counter the combined joint moments of the GRF and knee extensors, limb muscles place a net tensile stress on the dorsal aspect of the femur for most of the mid-portion of stance, when loading is highest (Fig. 5).

Force-platform data indicate that the femora of *T. merianae* are exposed to a combination of axial compression, bending and torsion. Maximum tensile and compressive stresses for each step occurred nearly simultaneously (Table 4; Fig. 6). Timing of peak stress was variable among individuals, but typically occurred after peak net GRF magnitude. At the time of peak stress, the GRF vector was oriented nearly vertically (Table 4; Fig. 6). The net plane of bending (i.e. angle of the neutral axis from the anatomical AP axis) shifts through time to reflect axial rotation of the femur; at the time of peak tensile stress (pooled mean: 39.1±2.5% contact), the anatomical dorsal cortex was in tension and the ventral cortex was in compression (Fig. 6). Because the GRF is essentially vertical for most of stance, shifts of the neutral axis indicate continuation of a similar absolute direction of bending through the course of femoral rotation during stance.

Peak tensile and compressive stresses averaged 8.6±0.4 and –13.5±0.7 MPa, respectively, across all three tegus; however, the fastest individual (tm04), with a locomotor speed over twice that of the other two individuals (1.6 *versus* 0.5 BL s^{-1}; Table 3), exhibited higher stresses (10.4±0.3 and –17.4±0.2 MPa; Table 4). Because axial compression (–3.4±0.1 MPa in the fastest individual; Table 4) is superimposed on bending during stance, peak compressive stresses are greater than peak tensile stresses. Femoral shear stress averaged 1.0±0.1 MPa across all three tegus and 1.3±0.2 MPa for the fastest individual (Table 4). As noted in the Materials and methods, these values (like those calculated for the species noted above) are minimum estimates that only account for torsion produced by the rotational moment exerted by the GRF.

Locomotor strain patterns

Because of constraints on the availability of animals of appropriate size for strain gauge implantation and their challenging behavior

Table 4. Mean peak stresses for femora of *T. merianae* with GRF magnitudes and orientations at peak tensile stress

Individual	Peak stress				Peak tension time (% contact)	Peak compression time (% contact)	Peak shear time (%)	Neutral axis angle from AP (deg)	Net GRF (BW)	GRF AP angle (deg)	GRF ML angle (deg)
	Tensile (MPa)	Compressive (MPa)	Axial (MPa)	Shear (MPa)							
tm04 (*N*=18)	10.4±0.3	–17.4±0.2	–3.4±0.1	1.3±0.2	37.7±4.0	32.6±3.9	34.2±3.5	16.0±1.4	0.48±0.04	2.3±3.5	–8.8±2.6
tm05 (*N*=16)	9.0±0.9	–13.8±1.4	–2.3±0.3	1.2±0.1	52.3±3.4	46.8±4.3	56.1±2.6	–1.1±6.7	0.34±0.02	6.5±2.4	–2.3±1.6
tm06 (*N*=15)	6.1±0.3	–8.6±0.4	–1.2±0.1	0.6±0.1	26.7±3.3	23.7±2.1	49.2±5.7	–12.6±2.2	0.40±0.02	11.7±2.0	–9.9±1.6
Mean	8.6±0.4	–13.5±0.7	–2.4±0.2	1.0±0.1	39.1±2.5	34.5±2.5	45.9±2.6	1.6±2.9	0.41±0.02	6.6±1.7	–7.0±1.3

Shear stresses are reported for clockwise rotations of the right femur as viewed from the proximal end.
Deviations of the neutral axis from the anatomical anteroposterior (AP) axis of each bone are clockwise in direction (i.e. negative angle from horizontal at 0 deg); use of this negative angle convention rather than those of our previous papers (Butcher and Blob, 2008a; Butcher et al., 2008) allows continuous plotting of values in Fig. 6 (e.g. a value of –10 deg in this paper would be equivalent to a value of 170 deg in the cited studies).
BW, body weight; ML, mediolateral.
Values are means ± s.e.m.; *N*, number of steps analyzed.

during experiments, only limited strain data could be collected. Differences in body size between individuals used in strain and force trials also place caveats on comparisons of these results. Though we acknowledge the limitations of our sample, we judged that the points of comparison that could be made between force and strain data made it preferable to report available strain data in the context of our current force-platform analyses, particularly given the rarity of bone loading data from lizards and the difficulty of obtaining

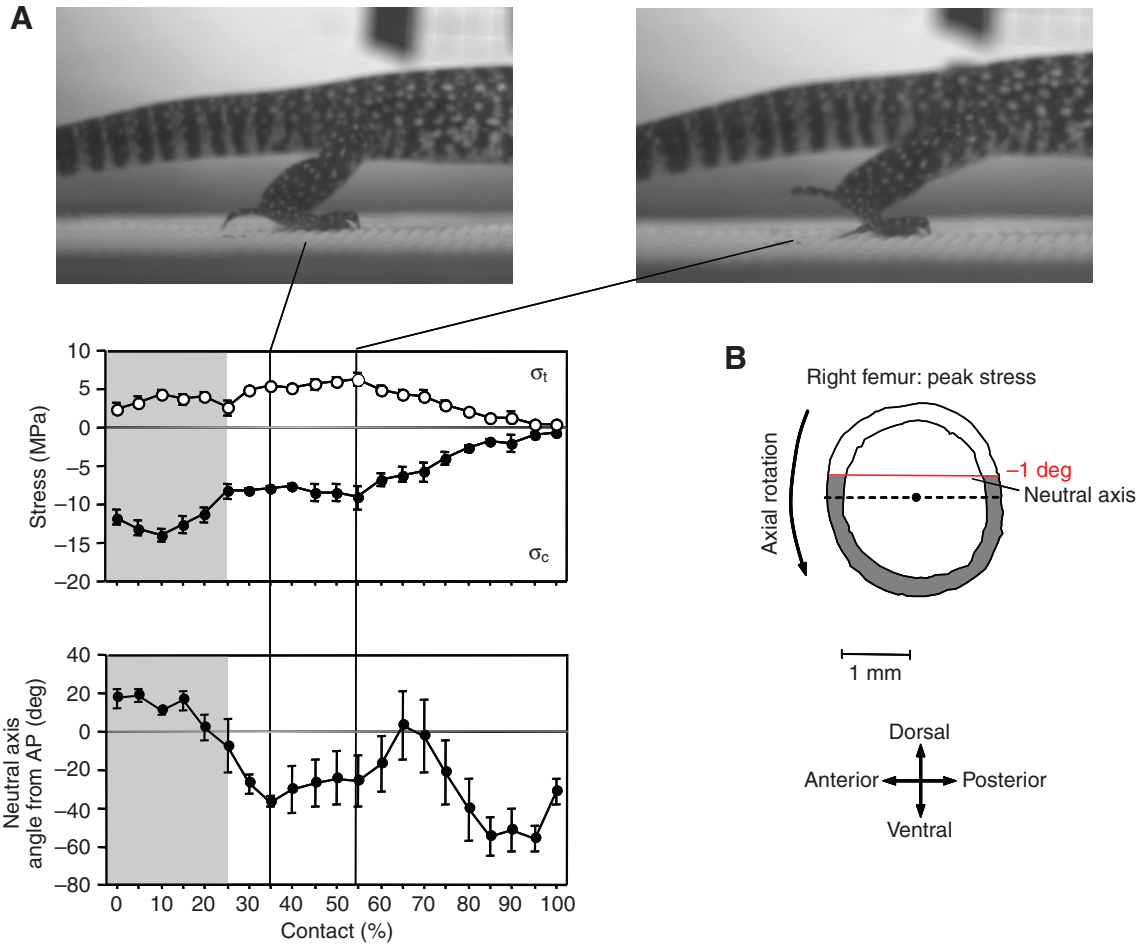

Fig. 6. (A) Maximum tensile (σ_t, open circles) and compressive (σ_c, filled circles) stresses acting in the right femur and neutral axis angle from the anatomical AP axis of the femur from an individual tegu. Plots show means ± s.e.m. over *N*=16 trials. Frame stills show limb position at the time of maximum GRF (left image) and maximum tensile stress (right image). Solid vertical lines mark the relative timing of these events. Grey shading over initial 25% of traces indicates the mean period of contact overlap between the forelimb and hindlimb for this individual. (B) Schematic cross-section of a right femur, illustrating the neutral axis orientation for bending (red line and value) at peak tensile stress. Portions of the femoral cortex experiencing compression are shaded, and portions experiencing tension are unshaded. Neutral axis is illustrated offset from the centroid (dark circle) because of axial compression superimposed on bending loads. The curved arrow (black) indicates the inward rotation of the femur during a step. Note that because the timing of peak tensile stress differs across trials, the value for mean neutral axis orientation at peak stress labeled for the cross-section (see Table 4) differs from that shown at the single time of mean peak stress indicated in the lower panel graph of A.

Table 5. Peak longitudinal (ε_{axial}), principal tensile (ε_t), principal compressive (ε_c) and shear strains recorded from the tegu femur during walking

Gauge site	ε_{axial} (με)	ε_t (με)	ε_c (με)	ϕ_t (deg)	Shear (με)
'Dorsal'	–237.9±14.3 (46, 2)*				
'Anterodorsal'	–208.0±6.1 (46, 2)*				
'Anterior'	115.4±7.6 (12, 1)	137.2±9.8 (12, 1)	–238.1±22.4 (12, 1)	33.2±1.1 (12, 1)	278.9±25.8 (12, 1)

*Grand means of strain for two animals.
Data are means ± s.e.m.; values in parentheses are the number of steps analyzed and the number of individuals tested, respectively.
ϕ_t, angle of principal tensile strain to the long axis of the bone; positive angles indicate inward (anterior) rotation.

data from the species we examined. Interpretations primarily based on strain analyses require caution in their consideration.

Generalizations about femoral strains in tegus during walking were made on the basis of the most common strain patterns observed for each recording site. Peak strain magnitudes were moderately variable between the two instrumented lizards (coefficients of variation averaged 27.9% across gauge locations). Unfortunately, ROS data were successfully recorded from the 'anterior' site of only one of the lizards (Table 5). Also, because of minor differences in gauge placement, recordings from the 'anterodorsal' site showed some variation between individuals as to the timing in the step when peak strains were tensile or compressive. However, patterns of tensile and compressive strain at each recording location were largely consistent between steps for each individual, allowing the general loading patterns of adult tegu femora to be interpreted from strain data.

Representative femoral strain patterns are shown in Fig. 7. Axial strain peaks from the 'dorsal' and 'anterior' locations were somewhat later than axial peaks from the 'anterodorsal' location and principal and shear peaks from the 'anterior' location, which occurred prior to midstance. 'Dorsal' axial strain records showed consistently compressive strains in both individuals. In contrast, the 'anterodorsal' and 'anterior' locations showed some shifts between tensile and compressive strains during the step, though the primary peaks for these locations were, respectively, compressive and tensile. In addition, tensile strains from the 'anterior' location were lower in absolute magnitude than those at the other two sites (Table 5; Fig. 7). These strain distributions, and the relative magnitudes of tension and compression around the cortex, corroborate results from force-platform trials indicating that the tegu femur is loaded in a combination of axial compression and bending.

Principal (and shear) strain traces typically showed only single maximum peaks, similar to observations during vigorous locomotion in other species ranging from reptiles (Blob and Biewener, 1999) to mammals (Rubin and Lanyon, 1982; Biewener and Taylor, 1986; Main and Biewener, 2004). Shear strain records confirm that, in

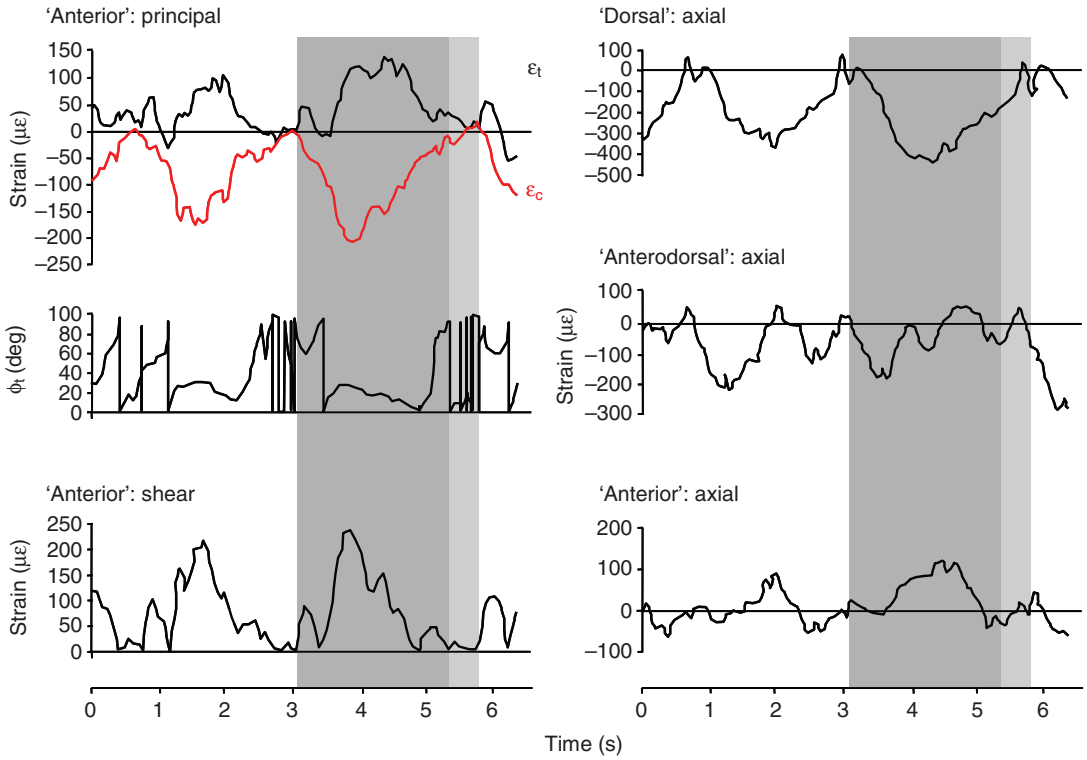

Fig. 7. Representative strain recordings (simultaneous) from three gauge locations on the femur during two consecutive walking steps from one individual tegu (tm01). Left: principal strains, angle of principal tensile strains from the femoral long axis (ϕ_t) and shear strains from ROS gauge recordings. Right: longitudinal strains from 'dorsal', 'anterodorsal' and 'anterior' sites. Note that strain scales differ among panels to facilitate presentation. Dark grey shading highlights the stance phase (contact) for a single step at all gauge locations. Light grey shading highlights the swing phase of a stride. ε_t and ε_c denote tensile and compressive (red line) principal strain traces, respectively.

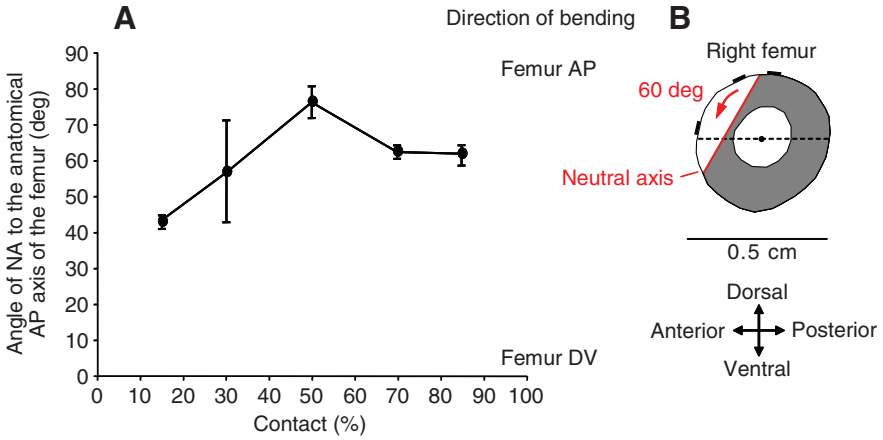

Fig. 8. (A) Shifts in the orientation of the neutral axis (NA) of femoral bending at five time increments (% contact) through the step for an individual tegu. Each data point represents the mean (±s.e.m.) angle of the NA to the anatomical anteroposterior (AP) axis of the femur averaged over *N*=5 steps. (B) Schematic femur cross-section illustrating NA orientation and shift. Strain gauge locations are indicated by the black bars around the cortex of the femoral cross-section. Solid red line is an NA with an orientation of 60 deg. Directions of bending are indicated with respect to the anatomical axes of the bone as described in the text, not in an absolute frame of reference. AP, bending about an NA running from the anatomical dorsal to ventral cortex; DV, bending about an NA running from the anatomical anterior to posterior cortex.

addition to bending and axial compression, tegu femora are subject to torsion. Mean orientations of peak principal tensile strain (ϕ_t) on the 'anterior' surface of the femur deviated from the long axis of the bone, with values averaging 33.2±3.9 deg (approaching the 45 deg value expected for torsional loading; Table 5; Fig. 7). Based on conventions for gauge configurations in our experiments, positive mean values for ϕ_t indicated counterclockwise (i.e. inward) rotation of the right femur (viewed from its proximal end) during the step. This orientation of torsional loading is the opposite of what would be predicted from GRF rotational moment data (see Fig. 4). This suggests that the net torsional loads experienced as strains on the femur must be produced by the contraction of the CFL and other retractor muscles against the rotational moment of the GRF (Reilly et al., 2005). Femoral shear strains in tegus exceeded mean peak principal strain measurements (compressive) by only 17% (Table 5; Fig. 7), somewhat lower than mean values reported for the femur in alligators and iguanas (Blob and Biewener, 1999).

Planar strain distribution analyses and neutral axis orientation

Planar strain analyses were conducted for the individual (tm01) for which we successfully recorded from all three recording sites, including the 'anterior' ROS gauge. Similar patterns emerged across trials through most of stance phase, though some variation in NA orientation was evident. At the beginning of the step, the NA was typically aligned near the anatomical AP axis, but shifted dorsal and anterior to the cross-sectional centroid (Figs 8, 9). As strain magnitudes increased through the step, the NA rotated in correspondence with the axial rotation of the femur, which tends to shift the 'dorsal' aspect of the femur to face somewhat 'anteriorly' in absolute space. By midstance and through the last half of the stance phase, strain distribution patterns indicated that the anterodorsal-to-anterior aspect of the femur was in tension and the ventral and posterior aspects were in compression. Although this NA orientation differed moderately from that indicated by force-platform analyses, the distribution of loading regimes around the femur generally matched well between the two analyses, with both indicating the presence of bending and axial compression, and showing ventral portions of the bone in compression and dorsal portions in tension. Through the last half of the step, the orientation of the NA was aligned diagonally between the anatomical AP and DV axes (Fig. 9), with peak axial strains occurring at 59.2±8.9% of contact.

Planar strain analyses indicate that peak tensile strains occur on the anterodorsal-to-anterior surfaces of the femur in tegus, and peak compressive strains occur on the posteroventral-to-posterior surfaces, rather than at the precise locations from which strains were recorded by attached gauges in the test animals. Based on the distribution of planar strain contours (Fig. 9), actual peak strains in the tegu femur are likely considerably higher than those recorded, averaging between 2.03× (tensile) and 4.54× (compressive) higher across trials in which planar strain distributions were calculated (*N*=10 steps).

Material properties and safety factor calculations

The pooled mean hardness value for femora from *T. merianae* (59.4±2.3; Table 6) produced a tensile yield stress value of 193.0±6.1 MPa and a tensile yield strain value of 7117±150 με in bending. Comparing yield stress values to the mean peak tensile stresses evaluated from tegu femora (8.6±0.4 MPa; Table 4) produces a safety factor in bending of 22.4 with a worst-case estimate of 11.5. However, comparison with the mean stress from the fastest individual (tm04: 10.4±0.3 MPa) produces a lower safety factor estimate of 18.6 (Table 6).

Before calculating strain-based safety factors for tegus, peak tensile principal strains (ε_t) recorded from tegu femora during locomotor trials were multiplied by 2.03 to reflect to results of planar strain analyses. Use of these data produced a tensile safety factor estimate for bending of 25.6. However, because planar strain analyses indicated much higher compressive strains than tensile strains for tegu femora (Fig. 9), we also calculated a bending safety factor estimate using peak compressive principal strains (ε_c). Accounting for tensile yield strains in bending typically being only 75% of compressive yield strains in bending (Biewener, 1993), we calculated a compressive yield strain of –9489 με and compared this with a functional strain value determined by multiplying mean ε_c (Table 5) by 4.54 (to reflect planar strain analyses). These calculations produced a safety factor estimate of 8.8 in bending (Table 7).

Each bone failed catastrophically in torsion, with yield and fracture occurring essentially simultaneously. Failure stresses and strains in torsion were moderate for femora (65.8±7.3 MPa, 9933.7±816.8 με, respectively) and higher for tibiae (78.7±14.4 MPa, 14,660.5±1910.7 με) (Table 8), although torsional stiffness at bone failure was slightly higher on average for femora *versus* tibiae (6.86±1.13 and 5.23±1.24 GPa, respectively; Table 8). Prior to safety factor calculations, peak functional shear strains recorded from tegu femora during locomotor trials were multiplied by 2.03 and 4.54 to reflect proportional increases in strain predicted by results of planar strain analyses (see above). This lower correction factor

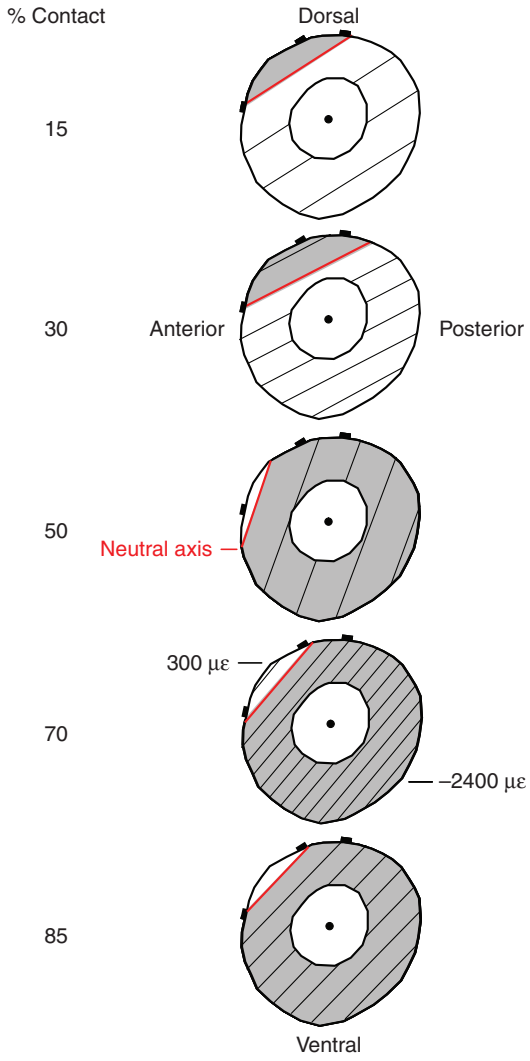

Fig. 9. Representative cross-sectional planar analyses of femoral strain distributions calculated for five time increments (% contact) during walking for an individual tegu. Time increments (% contact) correspond to those plotted in Fig. 8A. The centroid of each section is indicated by the black dot. Thin lines indicate contours of strain magnitude (all spaced at 200 με). Peak strains calculated for these steps are labeled at 70%. Compressive strains are shaded grey. The NA of bending (strain=0 με) is indicated by the red line (strain contour) separating compressive and tensile strains. Strain gauge locations are indicated by the black bars around the cortex of the femoral cross-sections. Anatomical directions are labeled and reflect the anatomical AP and DV axes illustrated in Fig. 8B.

in particular is similar in magnitude to the difference in shear magnitudes across recording sites in alligator femora (1.7×) moving at similar speeds (Blob and Biewener, 1999). Based on this range of strain magnitude corrections, safety factors in shear were determined to range between 7.8 and 17.5 (Table 8).

DISCUSSION

Loading regimes and magnitudes in tegu femora

Results from force-platform and strain analyses in tegus are consistent with those from salamanders and other studies of limb bone loading in sprawling tetrapods. For some aspects of our data (particularly *in vivo* strains) we have limited sample sizes of individuals from which to draw conclusions. Nonetheless, tegu

Table 6. Mechanical properties and stress-based safety factors for *T. merianae* femora in bending

N	Hardness (score)	Yield stress (MPa)	'Mean' safety factor
6	59.4±2.3	193.0±6.1	18.6–22.4*

Values are means ± s.e.m.
'Mean' safety factors were calculated as described in the text (see Materials and methods, Mechanical properties tests and safety factors).
*Lower value determined from stresses in fastest individual; higher value determined from mean stress across all individuals.

femora, like those of other sprawling tetrapods, including salamanders (Sheffield and Blob, 2011), iguanas and alligators (Blob and Biewener, 1999; Blob and Biewener, 2001) and turtles (Butcher and Blob, 2008a; Butcher et al., 2008), are exposed to a combination of axial compression, bending and torsion as a result of forces and moments imposed by the GRF and limb muscles, with the prominence of torsion distinctive compared with patterns seen in mammalian lineages with more upright limb posture.

The force-platform and strain analyses show a moderate difference in the orientation of bending, with force analyses generally showing closer alignment of the neutral axis with the anatomical AP axis of the femur (Figs 6, 8, 9). Some of the difference between the bending orientations evaluated in these studies may be related to the different sizes of tegus used for each type of analysis. For example, the larger tegus used in the strain studies may experience greater axial compression of the femur associated with their relatively larger mass, and might employ greater axial rotation of the femur that could dispose the neutral axis further from an AP alignment. However, our limited sample of strain data do corroborate results from force-platform analyses in that both studies showed the neutral axis to be shifted dorsally relative to the centroid of the femur, and both showed anterodorsal portions of the femur exposed to tension and posteroventral portions of the femur exposed to compression. These patterns match closely with the bending orientations and load distributions previously evaluated in turtles (Butcher and Blob, 2008a; Butcher et al., 2008) and salamanders (Sheffield and Blob, 2011), but differ from patterns reported for alligators and iguanas, in which tensile bending loads were shifted more anteroventrally in the femur (Blob and Biewener, 1999; Blob and Biewener, 2001). Thus, even among taxa that use patterns of sprawling limb kinematics that are (at least superficially) similar (including two species of lizard), there may be diversity in some aspects of limb bone loading mechanics. It is possible that relatively fine-scale differences in limb kinematics (e.g. extent of femoral rotation) could contribute to such loading diversity (Butcher and Blob, 2008a).

Like other sprawling tetrapods [e.g. iguanas (Blob and Biewener, 2001)], orientation of the GRF for tegu hindlimbs is nearly vertical for most of stance. At the time of peak stress (39.1±2.5% contact), the medial inclination angle of the GRF is 7.0 deg (Table 4), within the typical range of 3–13 deg observed in other sprawling taxa (Jayes and Alexander, 1980; Blob and Biewener, 2001; Butcher and Blob, 2008a). This small degree of medial GRF inclination is also similar to that seen in other animals with parasagittal limb posture (Biewener et al., 1983; Biewener et al., 1988). The similarity of GRF orientation at peak stress across the breadth of lineages, body sizes and locomotor patterns represented by taxa ranging from salamanders to turtles to lizards to horses gives a strong indication that differences in limb bone loading patterns across species can be primarily attributed to differences in limb position and its consequent

Table 7. Mechanical properties, estimated actual peak locomotor strains and strain-based safety factors for the femur of *T. merianae* in bending

Load	Yield strain bending (με)	Proportional strain increase	Peak calculated bending strain (με)	'Mean' safety factor bending
Tension	7117.0 (6)	2.03	278.5	25.6
Compression	–9489.0 (6)	4.54	–1081.0	8.8

Yield strain values are means calculated from hardness data as described in the text; values in parentheses are the number of bones analyzed.
Peak strain estimates were calculated based on planar strain distributions. These provided a quantitative measure of the proportional increases in recorded strains *versus* estimated strains.
'Mean' safety factor calculations are described in the text (see Materials and methods, Mechanical properties tests and safety factors).

orientation relative to the GRF, rather than on the absolute direction of the GRF.

One feature of femoral loading mechanics that sprawling tetrapods seem to have in common is that their patterns of limb motion place their femora at large angles to the GRF. In alligators and iguanas the femur is oriented over 60 deg from the GRF at peak stress (Blob and Biewener, 2001), and in salamanders (98.1±1.5 deg; Table 3) and turtles [89.6±1.1 deg (Butcher and Blob, 2008a)] the femur is nearly orthogonal to the GRF at the time of peak loading. This pattern is also observed in tegus, though the angle between the femur and the GRF at peak stress is somewhat larger than in previously studied sprawling species (111±3 deg). In all of these sprawling taxa, however, the near perpendicular orientation of the GRF to the long axis of the femur generates bending moments and stresses that are much larger than their axial counterparts (Fig. 5). One reason this angle might be larger in tegus than in other sprawling species is that peak stress in tegus usually occurs after peak GRF, whereas in other species it typically occurs before or nearly synchronous with peak GRF (Blob and Biewener, 2001; Sheffield and Blob, 2011). Thus, the spatial relationship between the GRF and the femur may differ between tegus and these other species because the tegu femur would be retracted further relative to the nearly vertical GRF by the time of peak stress.

Bending stresses calculated for the fastest juvenile tegu were similar to those found for salamanders [14.9±0.8 and –18.9±1.0 MPa (Sheffield and Blob, 2011)] and alligators [11.7±0.6 and –16.4±0.9 MPa (Blob and Biewener, 2001)], but lower than stresses reported for iguanas [27.1±2.1 and –37.0±2.8 MPa (Blob and Biewener, 2001)] or river cooter turtles [24.9±1.0 and –31.1±1.0 MPa (Butcher and Blob, 2008a)]. These studies of limb bone loading in sprawling animals also found significant torsion. In tegus, peak shear stresses from the fastest individual were 1.3±0.2 MPa (Table 4), moderately smaller than values seen in alligators [1.9±0.5 MPa (Blob and Biewener, 2001)], but considerably smaller than values from salamanders [4.1±0.3 MPa (Sheffield and Blob, 2011)], iguanas [5.8±2.8 MPa (Blob and Biewener, 2001)] or turtles [13.7±0.5 MPa (Butcher and Blob, 2008a)]. Elevated torsion has been predicted for species that drag a large tail on the ground, because the resistance to forward motion caused by the tail could impose a larger torsional moment on the hindlimb (Reilly et al., 2005). Results from this study correspond with others (Blob and Biewener, 2001; Butcher and Blob, 2008a; Sheffield and Blob, 2011) in showing that although dragging a tail may contribute to femoral shear stress, it is not the only factor that produces torsion. Instead, given that the highest levels of femoral torsion are actually seen in turtles, in which the tail is typically reduced and held off the ground (Willey and Blob, 2004), limb bone shear stress magnitudes are likely substantially affected by flexibility of the body axis (Butcher and Blob, 2008a; Butcher et al., 2008). Lateral body undulations may accommodate femoral twisting in many sprawling lineages, but for turtles with a rigid body axis, such torsional loads can only be resisted by the limbs (Butcher and Blob, 2008a; Butcher et al., 2008).

Although the GRF induces a rotational moment on the tegu femur that would tend to cause outward rotation (i.e. clockwise viewing the right femur from its proximal end), shear strains (reflecting the actual pattern of net loading on the bone) indicate inward rotation (i.e. counterclockwise viewing the right femur from its proximal end). Although our shear strains were measured from animals larger than those we used in our force-platform experiments, such inward rotation is expected based on the use of the CFL muscle as a limb retractor in lizards, as this muscle inserts on the ventral aspect of the femur and would tend to rotate the femur anteriorly as it shortens during retraction (Snyder, 1962; Gatesy, 1997; Blob, 2000). However, the opposing orientations of shear strains and GRF torsional moment data indicate that the net torsional loads experienced as strains on the femur must be produced by the contraction of retractor muscles against the rotational moment of the GRF. This mechanism for the production of femoral torsion is evident in alligators (Reilly et al., 2005) and is likely for iguanas, in which the GRF also induces outward rotational moments on the femur (Blob and Biewener, 2001). Although consistent across the lizard (and crocodilian) species that have been studied, this mechanism appears not to apply for salamanders (Sheffield and Blob, 2011) or turtles (Butcher and Blob, 2008a; Butcher et al., 2008), in which the rotational moment of the GRF induces inward rotation, complementing (rather than opposing) that produced by CFL retractor muscles. Thus, despite the superficially similar body plans and locomotor movements of many sprawling tetrapods, torsional loading of the femur appears to result from differing patterns of torsional moments across lineages, indicating that multiple functional paths can lead to similar ranges of functional performance (Wainwright et al., 2005; Blob et al., 2006).

Of the three tegus used in our force-platform trials, two walked very slowly (tm05: 0.4±0.05 BL s^{-1}; tm06: 0.6±0.04 BL s^{-1}; Table 4) whereas the third traveled more than twice as fast (tm04:

Table 8. Mechanical properties for the femur and tibia of *T. merianae* in torsion

Bone	Failure stress (MPa)	Failure strain (με)	Failure stiffness (GPa)	Peak calculated shear strain (με)	'Mean' safety factor shear
Femur	65.8±7.3 (4)	9933.7±816.8 (4)	6.86±1.13 (4)	566.2–1266.2	7.8–17.5
Tibia	78.7±14.4 (4)	14660.5±1910.7 (5)	5.23±1.24 (4)		

Data are means ± s.e.m.; values in parentheses are the number of bones analyzed.
Calculations of estimated peak shear strain values are described in the text (see Materials and methods, Mechanical properties tests and safety factors).

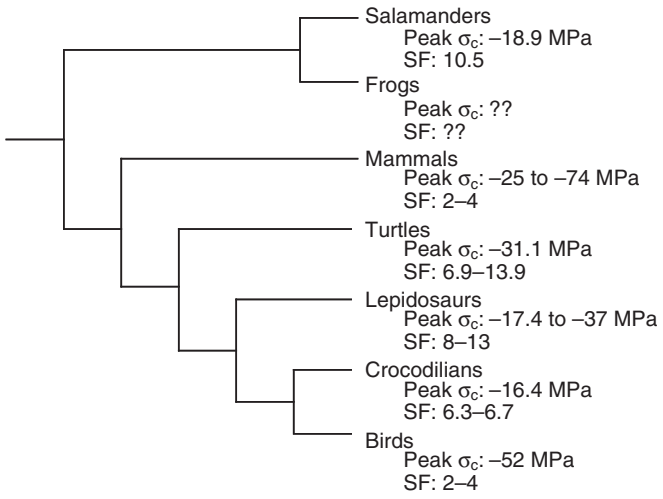

Fig. 10. Cladogram of tetrapod lineages mapping values of safety factors (SF) and peak compressive stresses (σ_c) in bending for hindlimb bones. All ectothermic taxa typically have higher safety factors than birds or mammals. Data are from the following sources: salamanders (Sheffield and Blob, 2011), turtles (Butcher and Blob, 2008a; Butcher et al., 2008), lepidosaurs (this study) (Blob and Biewener, 1999; Blob and Biewener, 2001), crocodilians (Blob and Biewener, 1999; Blob and Biewener, 2001), mammals and birds (Alexander, 1981; Biewener, 1991; Biewener, 1993).

1.6±0.47 BL s^{-1}; Table 3). This faster tegu (tm04) had similar timings of peak GRF when compared with the other two individuals, but had much higher tensile, compressive and axial stresses (tensile: 10.4±1.1 MPa; compressive: –17.4±0.9 MPa; axial: –3.4±0.1 MPa; Table 4). Shear stresses, in contrast, remained close to the values observed for the other two individuals (1.3±0.2 MPa), particularly the slowest tegu (tm05; Table 4). This indicates that speed effects may not be as prominent for shear stresses as they are for bending and axial stresses.

Safety factors in tegu femora: mechanical basis and evolutionary implications

Given the different speeds observed in force-platform trials, we calculated estimates of femoral safety factors in bending (Table 6) based on data from all three individuals (22.4) and based on data from just the fastest individual (18.6). For purposes of comparisons with other species, we feel that the safety factor calculated from the fastest individual provides the most appropriate value, because GRF magnitudes for this individual were over one-half body weight (Tables 3, 4), which is similar to what several other sprawling tetrapods (e.g. alligators, turtles) show at peak GRF and peak stress (Blob and Biewener, 2001; Butcher and Blob, 2008a). Femoral safety factors in bending based on *in vivo* strain measurements were calculated as 25.6 based on tensile strains, but only 8.8 based on compressive strains (Table 7). As other studies have noted (Biewener et al., 1983; Blob and Biewener, 2001; Butcher et al., 2008), some differences between stress- and strain-based safety factor calculations are not unexpected. In our comparisons of tegus, the differing methods used to elicit locomotion (overground *versus* treadmill) may have contributed to the differences between our stress- and strain-based estimates, as might the different sizes of animals used in the two sets of experiments. However, the upper ends of the ranges of values we determined from each technique correspond well, and both techniques place all estimates of femoral safety factors in bending for tegus well above limb bone safety factors typically calculated for birds and mammals (Alexander, 1981; Biewener, 1983a; Biewener, 1993). Instead, femoral safety factors in bending for tegus are more similar to the higher mean values reported for other sprawling, ectothermic tetrapods using either experimental method, including iguanas [8.0–10.8 (Blob and Biewener, 1999; Blob and Biewener, 2001)], alligators [6.3–6.7 (Blob and Biewener, 1999; Blob and Biewener, 2001)], river cooter turtles [6.9–13.9 (Butcher and Blob, 2008a; Butcher et al., 2008)] and salamanders [10.5 (Sheffield and Blob, 2011)]. Given the broadening range of reptilian and amphibian taxa in which high femoral safety factors have been observed, it appears likely that this is an ancestral condition from which lower limb bone safety factors evolved independently in birds and mammals (Fig. 10).

Although stress-based femoral safety factors in torsion are difficult to evaluate for tegus as only shear stresses induced by the GRF were calculated, available strain data indicated torsional safety factors between 7.8 and 17.5 (Table 8). These values are higher than previous torsional safety factors reported for reptiles such as iguanas and alligators [3.9–5.4 (Blob and Biewener, 1999; Blob and Biewener, 2001)] and river cooter turtles [3.1–3.8 (Butcher and Blob, 2008b; Butcher et al., 2008)]. As with our other conclusions based on our strain data from tegus, our estimates of torsional safety factors must be viewed cautiously given our limited sample size and the large body size of the animals we tested. However, all torsional safety factor estimates for lizards, crocodilians and turtles are still higher than those for endothermic taxa in which torsional loading is dominant [1.9 for the humerus of flying pigeons (Biewener and Dial, 1995)], again suggesting a trend for the evolution of lower limb bone safety factors in endothermic taxa. Such comparisons of safety factors for vigorous activities such as bird flight with less taxing walking by animals such as tegus and turtles may seem unfair in some respects if the behavior of the ectothermic taxa is simply not as demanding in the loads it imposes. Though it might be true that calculated safety factors for ectotherms might be lower if they simply performed more demanding behaviors, it still leaves open the question of why they maintain high safety factors in spite of frequently lower demands than experienced by mammals and birds.

Multiple factors may have contributed to the high limb bone safety factors seen in tegu lizards as well as other sprawling ectothermic tetrapods. First, natural selection may have selected against a low level of insurance in limb bones in these taxa if they were costly to grow or repair (Alexander, 1981; Lanyon, 1991; Diamond and Hammond, 1992; Diamond, 1998). Alternatively, the high safety factors seen in amphibians and non-avian reptiles may simply be an incidental consequence of selection acting on a wholly different trait, such as providing a sufficient surface area for the attachment of locomotor muscles (Blob and Biewener, 1999; Butcher and Blob, 2008a; Butcher et al., 2008). It is also possible that high limb bone safety factors are just ancestral conditions that are not disadvantageous enough to be selected against (Blob and Biewener, 1999). In this case, if high safety factors are an ancestral condition still found in amphibians and non-avian reptiles, then low safety factors in birds and mammals would be a convergent trait, rather than a widespread condition across all vertebrates. Given the phylogenetic position of tegus relative to other tetrapods studied, it seems that high limb bone safety factors are widespread in non-avian reptiles (Fig. 10). However, it also appears that there are several different paths to high safety factors, such as low limb bone loads or high bone strength (Sheffield and Blob, 2011). Further studies using representatives from unexamined clades would help to

document the scope of this diversity and provide insight into the evolution of limb bone design across tetrapods.

ACKNOWLEDGEMENTS

We thank C. Bridges, A. Sheffield, C. Gosnell and T. Maie for assistance with analysis, experiments and animal care; G. Rivera for construction of the trackway; A. Rivera for help with figures; and M. Ashley-Ross, A. Moran and two anonymous referees for reviewing drafts of the manuscript. J. DesJardins, T. Bateman, R. Thacker and N. Travis (Clemson Bioengineering) provided access to and generous assistance with mechanical testing equipment; D. Lieberman (Harvard) provided software for planar analysis of limb bone strains; and J. Walker (University of Southern Maine) provided access to software for data smoothing and normalization. Portions of this work were submitted as a Master's thesis at Clemson University by K.M.S. Support by NSF (IOB-0517340) and the Clemson Department of Biological Sciences are gratefully acknowledged.

REFERENCES

Alexander, R. McN. (1974). The mechanics of a dog jumping, *Canis familiaris*. *J. Zool. Lond.* **173**, 549-573.
Alexander, R. McN. (1981). Factors of safety in the structure of animals. *Sci. Prog.* **67**, 109-130.
Ashley-Ross, M. A. (1994). Metamorphic and speed effects on hindlimb kinematics during terrestrial locomotion in the salamander *Dicamptodon tenebrosus*. *J. Exp. Biol.* **193**, 285-305.
Biewener, A. A. (1982). Bone strength in small mammals and bipedal birds: do safety factors change with body size? *J. Exp. Biol.* **98**, 289-301.
Biewener, A. A. (1983a). Locomotory stresses in the limb bones of two small mammals: the ground squirrel and chipmunk. *J. Exp. Biol.* **103**, 131-154.
Biewener, A. A. (1983b). Allometry of quadrupedal locomotion: the scaling of duty factor, bone curvature and limb orientation to body size. *J. Exp. Biol.* **105**, 147-171.
Biewener, A. A. (1991). Musculoskeletal design in relation to body size. *J. Biomech.* **24 Suppl 1**, 19-29.
Biewener, A. A. (1992). *In vivo* measurement of bone strain and tendon force. In *Biomechanics – Structures and Systems: A Practical Approach* (ed. A. A. Biewener), pp. 123-147. New York: Oxford University Press.
Biewener, A. A. (1993). Safety factors in bone strength. *Calcif. Tissue Int.* **53 Suppl 1**, S68-S74.
Biewener, A. A. and Dial, K. P. (1995). *In vivo* strain in the humerus of pigeons (*Columba livia*) during flight. *J. Morphol.* **225**, 61-75.
Biewener, A. A. and Full, R. J. (1992). Force platform and kinematic analysis. In *Biomechanics – Structures and Systems: A Practical Approach* (ed. A. A. Biewener), pp. 45-73. New York: Oxford University Press.
Biewener, A. A. and Taylor, C. R. (1986). Bone strain: a determinant of gait and speed? *J. Exp. Biol.* **123**, 383-400.
Biewener, A. A., Thomason, J. J., Goodship, A. and Lanyon, L. E. (1983). Bone stress in the horse forelimb during locomotion at different gaits: a comparison of two experimental methods. *J. Biomech.* **16**, 565-576.
Biewener, A. A., Thomason, J. J. and Lanyon, L. E. (1988). Mechanics of locomotion and jumping in the horse (*Equus*): *in vivo* stress in the tibia and metatarsus. *J. Zool. Lond.* **214**, 547-565.
Blob, R. W. (2000). Interspecific scaling of the hindlimb skeleton in lizards, crocodilians, felids and canids: does limb bone shape correlate with limb posture? *J. Zool. Lond.* **250**, 507-531.
Blob, R. W. and Biewener, A. A. (1999). *In vivo* locomotor strain in the hindlimb bones of *Alligator mississippiensis* and *Iguana iguana*: implications for the evolution of limb bone safety factor and non-sprawling limb posture. *J. Exp. Biol.* **202**, 1023-1046.
Blob, R. W. and Biewener, A. A. (2001). Mechanics of limb bone loading during terrestrial locomotion in the green iguana (*Iguana iguana*) and American alligator (*Alligator mississippiensis*). *J. Exp. Biol.* **204**, 1099-1122.
Blob, R. W., Rai, R., Julius, M. L. and Schoenfuss, H. L. (2006). Functional diversity in extreme environments: effects of locomotor style and substrate texture on the waterfall-climbing performance of Hawaiian gobiid fishes. *J. Zool. Lond.* **268**, 315-324.
Butcher, M. T. and Blob, R. W. (2008a). Mechanics of limb bone loading during terrestrial locomotion in river cooter turtles (*Pseudemys concinna*). *J. Exp. Biol.* **211**, 1187-1202.
Butcher, M. T. and Blob, R. W. (2008b). Corrigendum: mechanics of limb bone loading during terrestrial locomotion in river cooter turtles (*Pseudemys concinna*). *J. Exp. Biol.* **211**, 2369.
Butcher, M. T., Espinoza, N. R., Cirilo, S. R. and Blob, R. W. (2008). *In vivo* strains in the femur of river cooter turtles (*Pseudemys concinna*) during terrestrial locomotion: tests of force-platform models of loading mechanics. *J. Exp. Biol.* **211**, 2397-2407.
Carrano, M. T. (1998). Locomotion of non-avian dinosaurs: integrating data from hindlimb kinematics, *in vivo* strains and bone morphology. *Paleobiology* **24**, 450-469.
Carter, D. R. (1978). Anisotropic analysis of strain rosette information from cortical bone. *J. Biomech.* **11**, 199-202.
Carter, D. R., Harris, W. H., Vasu, R. and Caler, W. E. (1981). The mechanical and biological response of cortical bone to *in vivo* strain histories. In *Mechanical Properties of Bone*, AMD Vol. 45 (ed. S. C. Cowin), pp. 81-92. New York: American Society of Mechanical Energy.
Dally, J. W. and Riley, W. F. (1978). *Experimental Strain Analysis*. New York: McGraw-Hill.
de Ricqlès, A. J. (1975). On bone histology of living and fossil reptiles, with comments on its functional and evolutionary significance. In *Morphology and Biology of Reptiles*, Linnean Society Symposium Series, Number 3 (ed. A. d'A. Bellairs and C. B. Cox), pp. 123-150. London: Academic Press.
de Ricqlès, A. J., Meunier, F. J., Castanet, J. and Francillon-Vieillot, H. (1991). Comparative microstructure of bone. In *Bone, Vol. 3, Bone Matrix and Bone Specific Products* (ed. B. K. Hall), pp. 1-78. Boca Raton, FL: CRC Press.
Demes, B., Qin, Y. X., Stern, J. T., Larson, S. G. and Rubin, C. T. (2001). Patterns of strain in the macaque tibia during functional activity. *Am. J. Phys. Anthropol.* **116**, 257-265.
Diamond, J. M. (1998). Evolution of biological safety factors: a cost/benefit analysis. In *Principles of Animal Design* (ed. D. W. Weibel, C. R. Taylor and L. Bolis), pp. 21-27. Cambridge: Cambridge University Press.
Diamond, J. M. and Hammond, K. A. (1992). The matches, achieved by natural selection, between biological capacities and their natural loads. *Experientia* **48**, 551-557.
Erickson, G. M., Catanese, J., III and Keaveny, T. M. (2002). Evolution of the biomechanical material properties of the femur. *Anat. Rec.* **268**, 115-124.
Estes, R., de Queiroz, K. and Gauthier, J. A. (1988). Phylogenetic relationships within Squamata. In *Phylogentic Relationships of the Lizard Families, Essays Commemorating Charles C. Camp* (ed. R. Estes and G. Pregill), pp. 119-281. Stanford, CA: Stanford University Press.
Furman, B. R. and Saha, S. (2000). Torsional testing of bone. In *Mechanical Testing of Bone and the Bone-Implant Interface* (ed. Y. H. An and R. A. Draughn), pp. 219-239. Boca Raton, FL: CRC Press.
Gatesy, S. M. (1997). An electromyographic analysis of hindlimb function in *Alligator* during terrestrial locomotion. *J. Morphol.* **234**, 197-212.
Gudynas, E. (1981). Some notes from Uruguay on behavior, ecology and conservation of the macroteiid lizard, *Tupinambis teguixin*. *Bull. Chicago Herpetol. Soc.* **16**, 29-39.
Hodgskinson, R., Currey, J. D. and Evans, G. P. (1989). Hardness, an indicator of the mechanical competence of cancellous bone. *J. Orthop. Res.* **7**, 754-758.
Irschick, D. J. and Jayne, B. C. (1999). Comparative three-dimensional kinematics of the hindlimb for high-speed bipedal and quadrupedal locomotion in lizards. *J. Exp. Biol.* **202**, 1047-1065.
Jayes, A. S. and Alexander, R. McN. (1980). The gaits of chelonians: walking techniques for very slow speeds. *J. Zool. Lond.* **191**, 353-378.
Lanyon, L. E. (1991). Biomechanical properties of bone and response of bone to mechanical stimuli: functional strain as a controlling influence on bone modeling and remodeling behavior. In *Bone, Vol. 3, Bone Matrix and Bone Specific Products* (ed. B. K. Hall), pp. 79-108. Boca Raton, FL: CRC Press.
Lieberman, D. E., Pearson, O. M., Polk, J. D., Demes, B. and Crompton, A. W. (2003). Optimization of bone growth and remodeling in response to loading in tapered mammalian limbs. *J. Exp. Biol.* **206**, 3125-3138.
Lieberman, D. E., Polk, J. D. and Demes, B. (2004). Predicting long bone loading from cross-sectional geometry. *Am. J. Phys. Anthropol.* **123**, 156-171.
Lowell, R. B. (1985). Selection for increased safety factors of biological structures as environmental unpredictability increases. *Science* **228**, 1009-1011.
Macey, J. R., Larson, A., Ananjeva, N. B. and Papenfuss, T. J. (1997). Evolutionary shifts in thee major structural features of the mitochondrial genome among iguanian lizards. *J. Mol. Evol.* **44**, 660-674.
Main, R. P. and Biewener, A. A. (2004). Ontogenetic patterns of limb loading, *in vivo* strains and growth in the goat radius. *J. Exp. Biol.* **207**, 2577-2588.
Main, R. P. and Biewener, A. A. (2007). Skeletal strain patterns and growth in the emu hindlimb during ontogeny. *J. Exp. Biol.* **210**, 2676-2690.
Peterson, J. A. and Zernicke, R. F. (1987). The geometric and mechanical properties of limb bones in the lizard, *Dipsosaurus dorsalis*. *J. Biomech.* **20**, 902.
Reilly, S. M., Willey, J. S., Biknevicius, A. R. and Blob, R. W. (2005). Hindlimb function in the alligator: integrating movements, motor patterns, ground reaction forces and bone strain of terrestrial locomotion. *J. Exp. Biol.* **208**, 993-1009.
Reilly, S. M., McElroy, E. J., Odum, R. A. and Hornyak, V. A. (2006). Tuataras and salamanders show that walking and running mechanics are ancient features of tetrapod locomotion. *Proc. R. Soc. B* **273**, 1563-1568.
Rubin, C. T. and Lanyon, L. E. (1982). Limb mechanics as a function of speed and gait: a study of functional strains in the radius and tibia of horse and dog. *J. Exp. Biol.* **101**, 187-211.
Sheffield, K. M. and Blob, R. W. (2011). Loading mechanics of the femur in tiger salamanders (*Ambystoma tigrinum*) during terrestrial locomotion. *J. Exp. Biol.* **214**, 2603-2615.
Snyder, R. C. (1962). Adaptations for bipedal locomotion in lizards. *Am. Zool.* **2**, 191-203.
Urban, E. K. (1965). Quantitative study of locomotion in teiid lizards. *Anim. Behav.* **13**, 513-529.
Wainwright, P. C., Alfaro, M. E., Bolnick, D. I. and Hulsey, C. D. (2005). Many-to-one mapping of form to function: a general principle in organismal design? *Int. Comp. Biol.* **45**, 256-262.
Wainwright, S. A., Biggs, W. D., Currey, J. D. and Gosline, J. M. (1976). *Mechanical Design in Organisms*. Princeton: Princeton University Press.
Willey, J. S. and Blob, R. W. (2004). Tail kinematics of juvenile common snapping turtles during aquatic walking. *J. Herpetol.* **38**, 360-369.
Wilson, M. P., Espinoza, N. R., Shah, S. R. and Blob, R. W. (2009). Mechanical properties of the hindlimb bones of bullfrogs and cane toads in bending and torsion. *Anat. Rec.* **292**, 935-944.